Trans Indian Inst Met (2019) 72(7):1721–1731
https://doi.org/10.1007/s12666-019-01639-7

TECHNICAL PAPER

Process Parameters Optimization of Friction Stir Welding of 6005A-T6 Aluminum Alloy Using Taguchi Technique

Zhongwei Ma[1] · Qinghua Li[1] · Lin Ma[1] · Wei Hu[1] · Bo Xu[2]

Received: 17 August 2018 / Accepted: 20 February 2019 / Published online: 11 March 2019

Abstract The control factors including rotating speed, welding speed and plunge depth of 6005A-T6 aluminum alloy friction stir welding were optimized by Taguchi method, and the combined effects of these factors were comprehensively investigated. Statistical results were analyzed by the analysis of variances and signal-to-noise ratios. The results show that the rotating speed is the most dominant factor in determining the joint tensile strength; and the plunge depth and welding speed are the second and third effective parameters, respectively. Under the optimum process parameters, the joint maximum tensile strength reaches 239.6 MPa which is 84% of that of the base material. The relationships between the main control factors, thermal cycle, formation, microstructure, mechanical properties and fracture characteristics were investigated.

Keywords Friction stir welding · Taguchi method · 6005A-T6 aluminum alloy · Microstructure · Mechanical properties

Zhongwei Ma and Qinghua Li contributed equally to this work.

✉ Lin Ma
mlin128@163.com

✉ Wei Hu
huwei201805@126.com

[1] Shenyang Aerospace University, No. 37 Daoyi South Avenue, Daoyi Development District, Shenyang 110136, China

[2] Bombardier Sifang (Qingdao) Transportation Ltd., 86 Jinhong Dong RD, Chengyang District, Qingdao 266111, China

1 Introduction

Friction stir welding (FSW), a rather recent solid-state welding method, was invented by The Welding Institute (TWI) in 1991 [1–4]. During the FSW process, the peak welding temperature is lower than melting point of the welded materials and the defects existing in the traditional fusion welding methods, such as porosity, hot crack and large deformation can be avoided [5–7]. Because of the advantages mentioned above, FSW can be applied to joining metals with low melting point, such as aluminum, magnesium and their alloys [8–12].

Due to the medium strength, excellent extrusion performance and good corrosion resistance, 6005-T6 aluminum alloy is widely used in the railway carriages which have an imperative demand of lighter and more economical structures. The investigation of FSW on 6005-T6 alloy has been become a hotpot in recent years. Meng et al. [13] found that although increasing rotating speed was beneficial in avoiding the cavity defect in the stir zone (SZ) of the FSW joint, the increased heat input decreased the joint microhardness and enlarged the joint softening region. Ji et al. [14] performed stationary shoulder FSW of 6005A-T6 alloy and found that the tensile strength of the joint was first increased and then decreased when the welding speed varied from 100 to 600 mm/min. In fact, 6005A-T6 Al is an age-hardening alloy. Therefore, the SZ, thermo-mechanically affected zone (TMAZ) and heat-affected zone (HAZ) of the joint are inevitably softened by the welding heat during FSW process. The softening regions are the weak part for the joint, and the fracture always occurs at these regions. Dong et al. [15] has reported that the peak temperature played an important role in the joint softening, which was influenced by various process parameters. Although there are considerable literatures about the FSW

of 6005-T6 alloy [15–17], most of them only changes one single process parameter during the investigation. Since the influence of process parameters on the joint quality is combined, studying the relationship between one single parameter and joint quality cannot acquire accurate and systematic conclusions. Therefore, the systematic investigation on the relationships between the main process parameters and joint quality is significant for enriching the technical storage and engineering application of FSW on 6005A-T6 alloy.

Since the final quality of joint depends on various parameters of FSW process, a series of reasonable experiments are essential to determine the optimum parameters. Generally, classical process parameter designs require many experiments to determine the optimum parameters, which are difficult, time consuming and expensive [18]. Taguchi method, a robust experimental design method, was developed by Taguchi and Konishi and widely used in engineering analysis to optimize the process parameters [19]. Compared with the classical experimental designs, the Taguchi method takes attention on the variance minimization of the interest characteristic. Therefore, the optimum range of parameters can be acquired efficiently by relatively few experiments [20]. The optimizing process of Taguchi method consists of six stages, as follows: (1) identifying the quality characteristic to be optimized; (2) determining the control factors of quality characteristic and their alternative levels; (3) selecting an appropriate orthogonal array (OA); (4) conducting the experiment based on the configured OA; (5) analyzing the data by signal-to-noise ratios (S/N) and analysis of variances (ANOVA) and determining the optimum parameters; (6) verifying the optimum parameters through validation experiments.

Taguchi method has been applied in the parameter optimization of FSW process. However, no literature on applying Taguchi method on 6005A-T6 alloy FSW has been reported so far. In this study, in order to acquire a better understanding of the relationships of parameters-microstructures-properties, the Taguchi method was used to optimize the process parameters of 6005A-T6 alloy FSW and the experimental results were analyzed by S/N and ANOVA. The relationships of process parameters, microstructures and mechanical properties were systemically discussed.

2 Experimental Procedure

The material used in the present study was 6005A-T6 aluminum alloy with the dimensions of 200 mm × 80 mm × 3 mm. The welding tool consisted of a six-groove shoulder with a 10 mm diameter and a conical screw thread pin with a 2.7 mm length. The pin tip and pin bottom diameters were 3 mm and 5 mm, respectively.

The NiCr–NiSi K-type thermocouples were used as temperature measurement instruments and placed in the joint retreating side (RS) with a distance of 1 mm from the weld edge to record the temperature history during FSW process. Before welding, all the plates were cleaned by sandpapers. After welding, the joints were cut perpendicular to the welding direction to prepare metallographic specimens. Before the observation, samples were polished and then etched by Keller reagent. The optical microscope (OM, OLYMPUS GX51) was used to examine the microstructure. In order to measure the microhardness distribution of joint cross section, the Vickers microhardness test was performed by the test machine (THV-1MD) at the load of 200 g for 10 s, and the distance between the tested points was 0.5 mm. The tensile test was carried out by the testing machine (SHIMADZU EHF-UV200K2) at room temperature according to ISO 4136:2001 at a cross-head speed of 3 mm/min. The schematic diagram of the specimen is shown in Fig. 1. The fracture surfaces were analyzed by the scanning electron microscope (SEM, SU3500) equipped with an energy-dispersive spectrometer (EDS).

3 Taguchi Method

3.1 FSW Parameters

As the control factors of FSW process, the welding speed, rotating speed and plunge depth play essential roles in the control of the heat input and material flow, thereby influencing the microstructural evolution and mechanical properties of the FSW joint. Actually, the literatures on the comprehensive investigation of 6005A-T6 alloy prepared by FSW by optimizing these factors are limited. Based on the earlier stage of present study, the level values of the control factors are selected and the results are listed in Table 1. According to the confirmed control factors and levels, an orthogonal array of L_9 is used (Table 1).

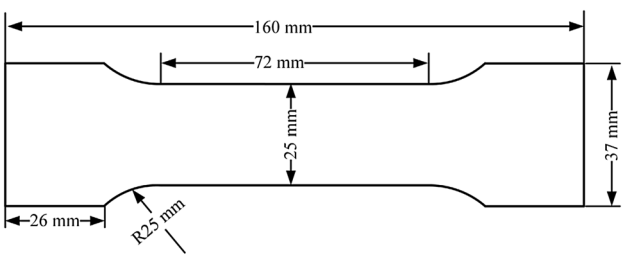

Fig. 1 Schematic of tensile specimen

Table 1 Process parameters and their levels

Level	Control factors		
	A Rotating speed (rpm)	*B* Welding speed (mm/min)	*C* Plunge depth (mm)
1	1100	350	0.1
2	1300	550	0.2
3	1500	750	0.3

3.2 Signal-to-Noise Ratio

This study aims to evaluate the relationships between the process parameters (control factors) and the joint tensile strength (quality characteristic). The mean value and S/N of the quality characteristic are used to assess the relationships. The 'S (signal)' and 'N (noise)', respectively, represent the mean desirable value and undesirable value of the output quality characteristic. Therefore, the ratio of the mean to square deviation can be expressed as the S/N ratio which represents the deviation degree of the quality characteristic from the desired value. Three categories of performance can be used to analyze S/N ratio: the lower the better, the nominal the better and the higher the better. In order to acquire the maximum tensile strength, the category of 'the higher the better' is used. Thus, the S/N ratio η_{ij} can be acquired by the following formula:

$$\eta_{ij} = -10 \log\left(\frac{1}{n}\sum_{j=1}^{n}\frac{1}{y_{ij}^2}\right)$$

where y_{ij} is the tensile strength of the ith experiment at the jth test and n is the test number of each experiment. The mean values and S/N ratios of the tensile strength under each parameter combination are presented in Table 2.

As the characteristic of orthogonal experimental design, the effect of each control factor at different levels can be separately analyzed. As a result, the average mean and S/N ratio value of each control factor under different levels are presented in Table 3. This table is the response table of the average mean and S/N ratio for the quality characteristic. The main effects of them are plotted in Fig. 2a, b to illustrate the responses. The change trends of average mean and S/N ratio values over the same factors are similar. From Fig. 2, the effects of factor level on response characteristic can be achieved. The higher average S/N ratio corresponds to the higher joint tensile strength. For example, Fig. 2 presents that the average S/N ratio first increases and then decreases with the level of B increasing from level 1 to level 3. It means that the joint tensile strength experiences an increase and then a decrease with the welding speed increasing from 350 to 750 mm/min. Therefore, the optimum level of welding speed is 550 mm/min. Likewise, the optimum parameter combination is $A_3B_2C_2$ which means the rotating speed of 1500 rpm, welding speed of 550 mm/min and plunge depth of 2 mm.

3.3 ANOVA

ANOVA is performed to quantify the effect of control factors on the quality characteristic. This analysis is accomplished by separating the total variability of the S/N ratios into contributions by each process parameters and the residual error. The sum of the squared deviations from the total mean S/N ratio is used to measure the total variability of the S/N ratios [18, 19]. F test is used to assess the effective degree of the process parameter on the quality characteristic. Generally, the change of the corresponding control factor has a significant effect on the quality characteristic when the F value is higher than 4 [21]. Tables 4 and 5 show the ANOVA results of mean and S/N ratio,

Table 2 Experimental layout: L_9 orthogonal array, tensile strength and S/N ratio

Experiment no.	Control factors			Mean tensile strength (MPa)	S/N ratio
	A	*B*	*C*		
1	1100	350	0.2	220.1	46.82777
2	1100	550	0.3	224.2	47.00147
3	1100	750	0.1	203	46.14655
4	1300	350	0.3	208.1	46.36610
5	1300	550	0.1	212.7	46.55310
6	1300	750	0.2	213.1	46.57104
7	1500	350	0.1	217.7	46.75517
8	1500	550	0.2	239.6	47.58987
9	1500	750	0.3	232.2	47.36098

Table 3 Response table of means and S/N ratios

Level	Means (MPa)			S/N ratios		
	A	*B*	*C*	*A*	*B*	*C*
1	216	215	211	46.65859	46.64968	46.48494
2	211	225	224	46.49675	47.04814	46.99623
3	230	217	221	47.23534	46.69286	46.90952
Delta	19	10	13	0.74	0.40	0.512
Rank	1	3	2	1	3	2

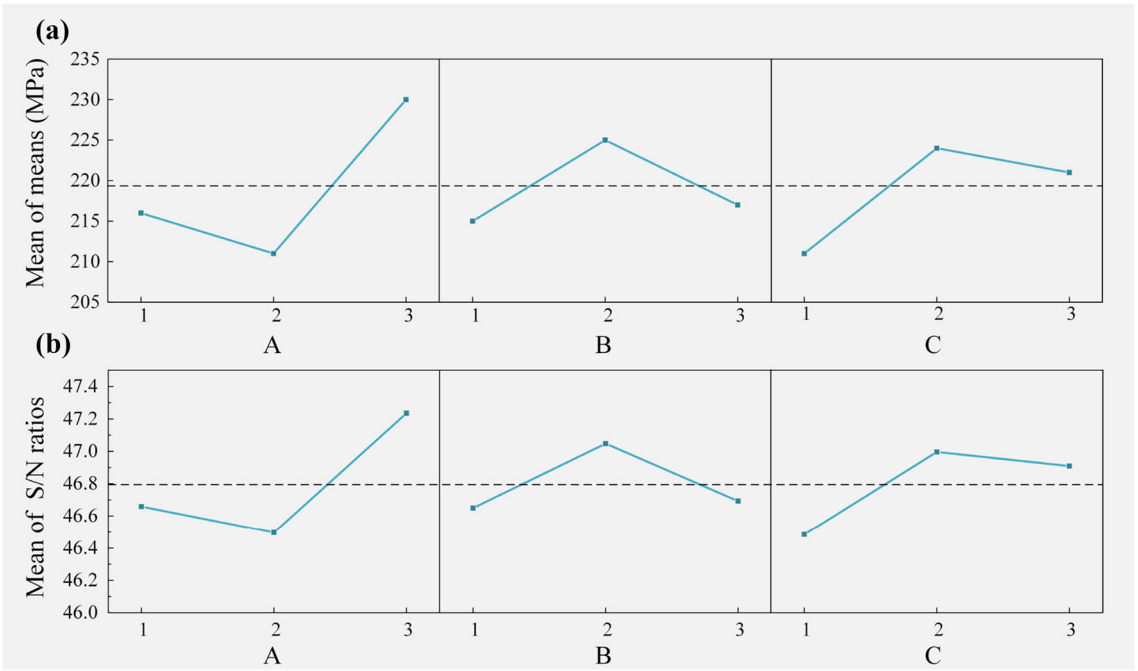

Fig. 2 Main effect plots for **a** means and **b** S/N ratios

respectively. It is shown that the F values of the rotating speed, welding speed and plunge depth are all higher than 4, which indicates that all the three process parameters are the highly significant control factors for the joint tensile strength. The contributions of the control factors on the tensile strength are different. The rotating speed has the largest contribution, which indicates that the rotating speed is the most dominant factor for the joint tensile strength among the three parameters in this study.

Generally, as the final process, a confirmation experiment should be performed to verify the optimum parameter combination, which can be omitted in this study since the optimum parameter combination (No. 8, Table 2) has been identified in the nine performed experiments. The maximum tensile strength is 239.6 MPa which reaches 84% of that of base material (BM).

4 Results and Discussion

The fabrication of FSW joint contains a coupling process of temperature and flow fields, which is predominantly controlled by the process parameters. There are complex relationships between heat input, material flow, metallurgical and mechanical properties. For example, an increased rotating speed leads to the increased heat input and material flow, thereby leading to the variation in the metallurgical and mechanical properties. Based on the experiment results of the Taguchi method, a detailed discussion on the effects of major control factors (welding speed, rotating speed and plunge depth) on the thermal cycles and metallurgical and mechanical characteristics of FSW joints are presented as follows.

Table 4 ANOVA results based on mean

Source	*Dof*	Seq SS	Adj MS	*F*	Contribution (%)
A	2	593.0020	296.50099	14.51486	53.2
B	2	188.4012	94.20058	4.61148	16.9
C	2	292.5742	146.28711	7.16131	26.1
Residual error	2	40.8548	20.42741	–	3.7
Total	8	–	–	–	100

Dof degrees of freedom, *Seq SS* sequential sum of squares, *Adj MS* adjusted mean square, *F* Fisher ratio

Table 5 ANOVA results based on S/N ratio

Source	*Dof*	Seq SS	Adj MS	*F*	Contribution (%)
A	2	0.9043	0.45217	12.89873	52.9
B	2	0.2869	0.14343	4.09157	16.8
C	2	0.4492	0.22460	6.40702	26.3
Residual error	2	0.0701	0.03506		4.0
Total	8	–	–	–	100

4.1 Thermal Cycles

The joint formation and microstructure are mainly related to the thermal cycle during welding process. The heat input is associated with the friction heat induced by the friction action between the tool surface and BM, as well as the deformation plastic heat. The peak temperatures under different parameters are presented in Fig. 3. Figure 3a–c presents the thermal cycles under the plunge depths of 0.1 mm, 0.2 mm and 0.3 mm, respectively. The ANOVA results indicate that the welding speed and rotating speed are the main control factors of the joint quality. The ratio of rotating speed to welding speed is represented by *w*/*v* which is investigated as a main factor influencing the joint quality in many papers [22–24]. The temperature curves present a similar change in trend. When the rotating tool approaches and then gets away from the measured point, the temperature experiences a sharp increase and then a relatively slow decrease. It is found that the peak temperature is increased with the increase of the *w*/*v* value under the same plunge depth. The highest peak temperature is 327 °C which is acquired under the rotating speed of 1300 rpm, welding speed of 350 mm/min and plunge depth of 0.3 mm (Fig. 3c). It is noteworthy that the highest *w*/*v* value is the parameter combination of 1500 rpm, 350 mm/min (Fig. 3a), while the peak temperature under this combination is not the highest one due to the small plunge depth (0.1 mm). Therefore, the plunge depth is also a main control factor for the heat input during welding process. Figure 3c shows that under the welding speed of 550 mm/min and 750 mm/min, the parameter combinations have the same *w*/*v* ratio value of 2. However, the peak temperature under the low welding speed is 295 °C which is a little higher than that under the high welding speed. It is because, the low welding speed increases the time of preheating effect on the region to be welded, which is beneficial in increasing the peak temperature. In fact, the welding process is also an annealing process for the joint material [25]. A higher welding speed results in a shorter thermal cycle and a lower peak temperature, which limits the grain growth. Moreover, the excessively low heat input always leads to an insufficient material flow and the excessively high heat input always results in a high softening degree of the joint. Under the optimum parameter combination, the peak temperature of 281 °C is a middle level among the nine parameter combinations. A proper heat input is one of key factors for the acquirement of the joint with high tensile strength.

4.2 Formations

The typical joint formations under different parameter combinations are displayed in Fig. 4. It is shown that the distance between the shoulder marks decreases when the *w*/*v* ratio increases from 1.7 to 3.1. The decreased distance results in a smoother joint surface. The amount and volume of flashes also increases with the increase of *w*/*v* ratio. The increased *w*/*v* ratio leads to the increase of peak temperature (Fig. 3), which is propitious to the improvement of material plasticity. Therefore, more material flows out from

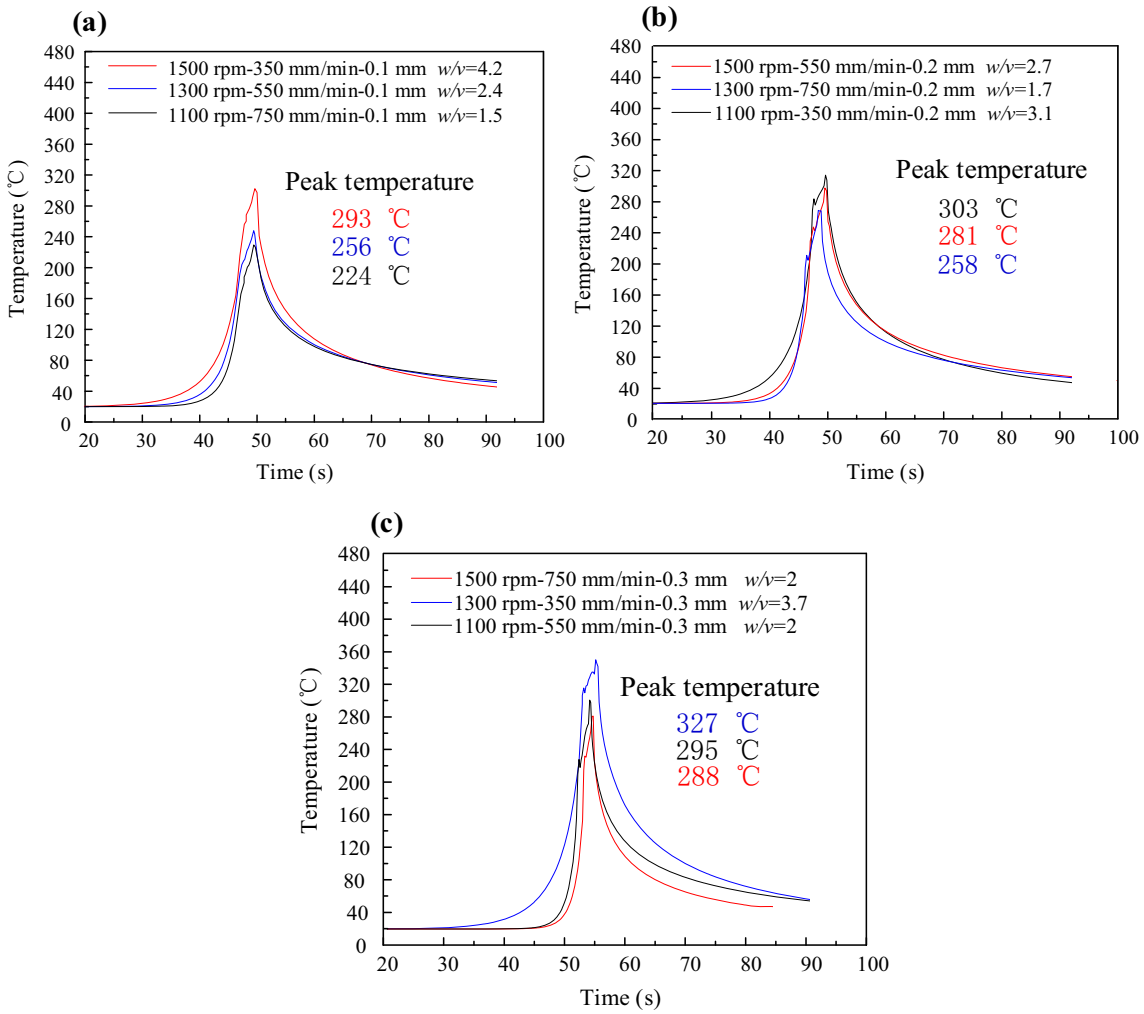

Fig. 3 Thermal cycles under different plunge depths: **a** 0.1 mm, **b** 0.2 mm and **c** 0.3 mm

the edge of the tool shoulder and forms larger flashes. The comparisons of Fig. 4a, c, e show that with the plunge depth varying from 0.1 to 0.3 mm, the amount of flashes has an obvious increase because of the higher peak temperature and more material being extruded out from the weld. Although the *w*/*v* ratio in Fig. 4e is relatively high, the amount of flashes is the smallest one due to the smallest plunge depth. The formation of flashes at the weld edge is the main reason to induce the joint thickness reduction which is a main factor influencing the joint tensile properties [26]. The thickness reduction can reduce the load-bearing capacity of the joint and increase the stress concentration at the weld edge, which causes the decrease of joint tensile strength.

4.3 Microstructures

Figure 5 shows the morphologies of the joint cross sections under different parameter combinations. Figure 5b–d display the joint cross section obtained under the plunge depth of 0.2 mm. A cavity can be observed in the joint cross section at the *w*/*v* ratio of 1.7 because of the insufficient material flow under low heat input (Fig. 5b). The cavity defect disappears and the widths of the SZ bottom, respectively, increase from 2.81 to 3.17 mm and 3.43 mm when the *w*/*v* ratio increases from 1.7 to 2.7 and 3.1. The enlarged SZ indicates the increased material flow in the SZ. Under the condition in Fig. 5b, the heat input is insufficient and the stir action of the tool is weak, resulting in an insufficient flow of plasticized material. The cavity and tunnel defects are likely to occur when the position behind the tool cannot be refilled by the material.

Figure 5a, c, e displays the joint cross section under the plunge depths of 0.1 mm, 0.2 mm and 0.3 mm, respectively. Compared with Fig. 5b, the cross section in Fig. 5e has a bigger *w*/*v* ratio and the cavity defect disappears in the SZ. Although the *w*/*v* ratios of the joints in Fig. 5e is higher than that in Fig. 5a, c, the small plunge depth of

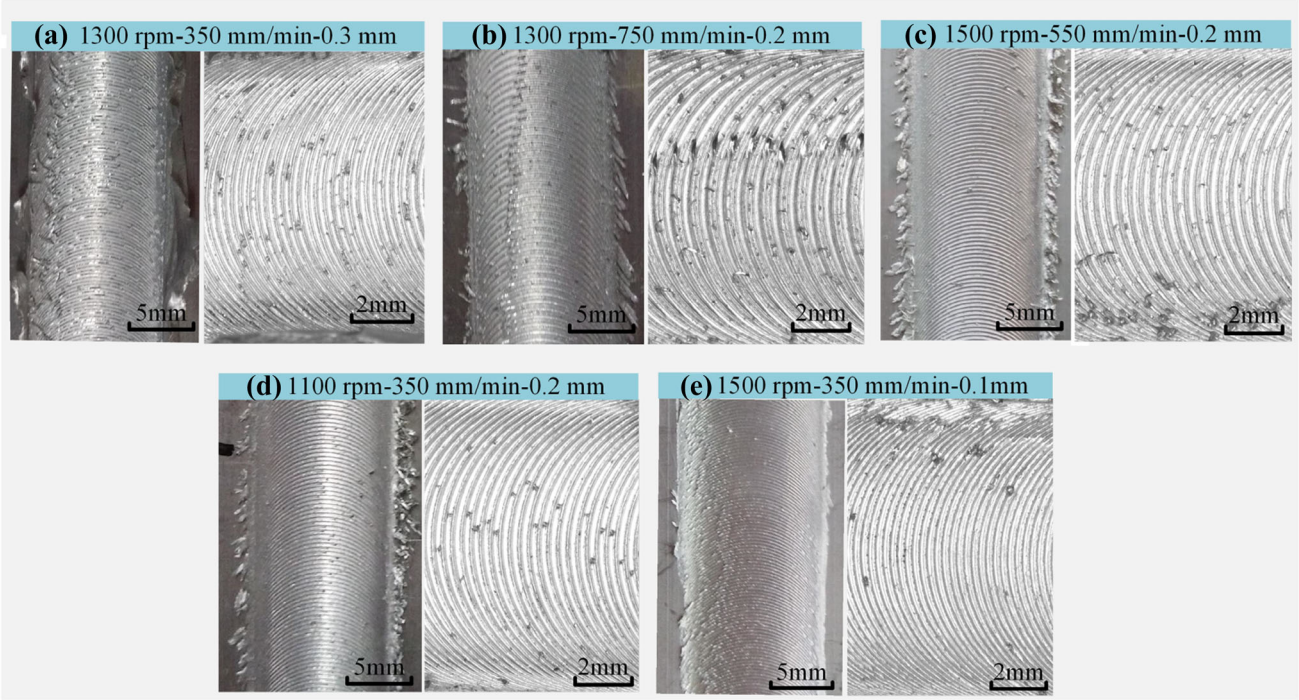

Fig. 4 Joint surface formations under different parameter combinations: **a** 1300 rpm-350 mm/min-0.3 mm, **b** 1300 rpm-750 mm/min-0.2 mm, **c** 1500 rpm-550 mm/min-0.2 mm, **d** 1100 rpm-350 mm/min-0.2 mm and **e** 1500 rpm-350 mm/min-0.1 mm

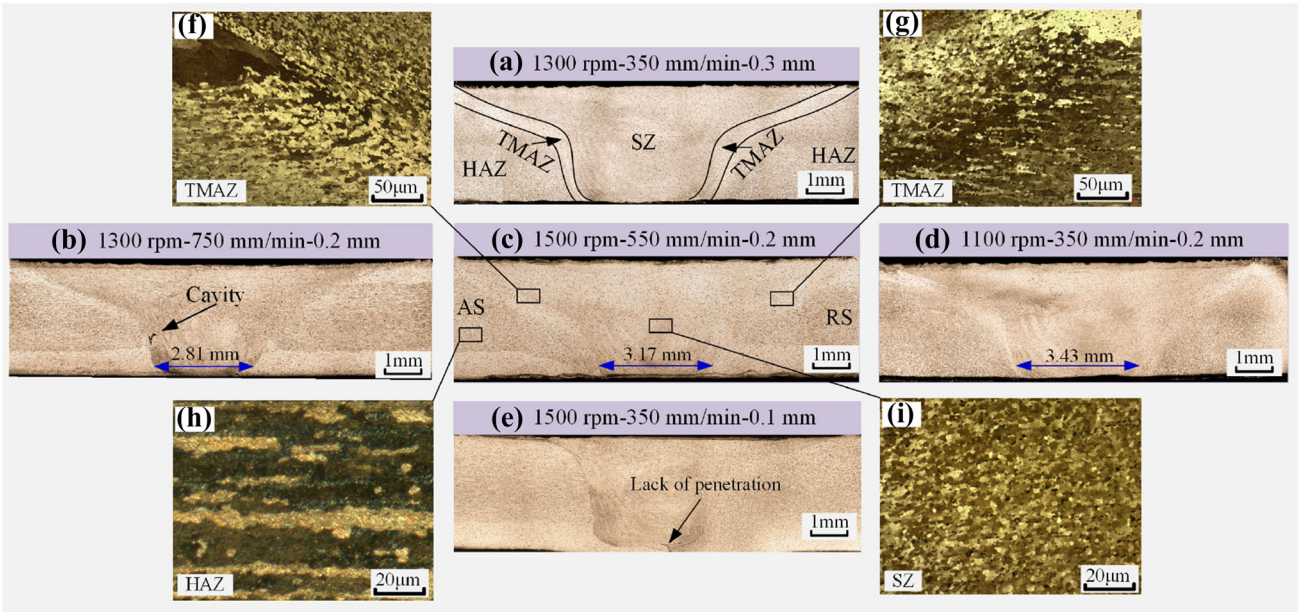

Fig. 5 Joint cross sections: **a** 1300 rpm-350 mm/min-0.3 mm, **b** 1300 rpm-750 mm/min-0.2 mm, **c** 1500 rpm-550 mm/min-0.2 mm, **d** 1100 rpm-350 mm/min-0.2 mm and **e** 1500 rpm-350 mm/min-0.1 mm; microstructures under different regions: **f** TMAZ in AS, **g** TMAZ in RS, **h** HAZ and **i** SZ

0.1 mm leads to the appearance of lack of penetration at the joint bottom (Fig. 5e). These results illustrate that the appearance of lack of penetration defect is sensitive to the plunge depth. Firstly, the low heat input induced by the small plunge depth results in an insufficient material flow around the pin tip. Secondly, the small plunge depth results

in a relatively big distance between the pin tip of the tool and the bottom surface of plate. Lastly, Janaki et al. [27] reported that the axial force decreases with the decrease of plunge depth. Therefore, the small plunge depth cannot provide enough forging force during the welding process, which is adverse to the atom diffusion. These three reasons lead to the formation of lack of penetration defects in the joint bottom. In fact, the lack of penetration can be avoided by increasing the *w*/*v* ratio to increase the material flow near the pin tip under the small plunge depth of 0.1 mm. However, the increased *w*/*v* ratio also leads to a higher heat input, which increases the softening degree of the joint and is detrimental to the joint tensile strength. Therefore, compared with the plunge depths of 0.1 mm and 0.3 mm, the plunge depth of 0.2 mm is a proper parameter which is beneficial in avoiding the lack of penetration defect and reducing the loss of the joint tensile strength in this study.

The joint cross section can be divided into SZ, TMAZ, HAZ and BM according to the microstructural characteristics (Fig. 5a) [28]. The SZ consists of fine-equiaxed grains resulting from the dynamic recrystallization induced by the intense stirring action of the tool and the thermal effect during the welding process [29] (Fig. 5i). The grains in the TMAZ are elongated and bended due to the plastic deformation (Fig. 5f, g). Compared with the relatively clear and narrow boundary between the TMAZ and SZ in advancing side (AS) (Fig. 5f), the boundary in RS (Fig. 5g) presents a diffused morphology, which results from the differences in force condition and thermal cycle between AS and RS. Moreover, the width of the TMAZ in RS is bigger than that in AS, resulting in a smoother microstructural transition between the TMAZ and HAZ. Since the grains in the HAZ only experience the thermal cycle and no plastic deformation occurs in this zone (Fig. 5h), the grain structure is similar to that in BM and the grain size is increased.

The enlarged views of the top, middle and bottom region of SZ under different parameters are displayed in Fig. 6. The grain size presents a decreasing trend from the SZ bottom to SZ top. The heat input at the SZ top is higher than that at the SZ bottom due to the friction between the tool shoulder and the plate top surface. Additionally, the thermal conductivity at the joint top surface is smaller than that at the joint bottom surface due to the application of metal backing plate. These two reasons respectively provide more energy and longer high temperature exposure time for the grain growth at the SZ top, thereby resulting in the coarser grains. The grain sizes at the SZ top, middle and bottom are all increased with the increase of *w*/*v* ratio, which is because, the increased heat input induced by the higher *w*/*v* ratio facilitates the grain growth.

4.4 Microhardness Distributions

The microhardness distributions in the joint cross sections are investigated. The measured points are 1.5 mm away from the joint top surface. Figure 7 presents the microhardness distributions of the joints with the highest (1300 rpm, 350 mm/min and 0.3 mm) and lowest (1100 rpm, 750 mm/min and 0.1 mm) peak temperatures

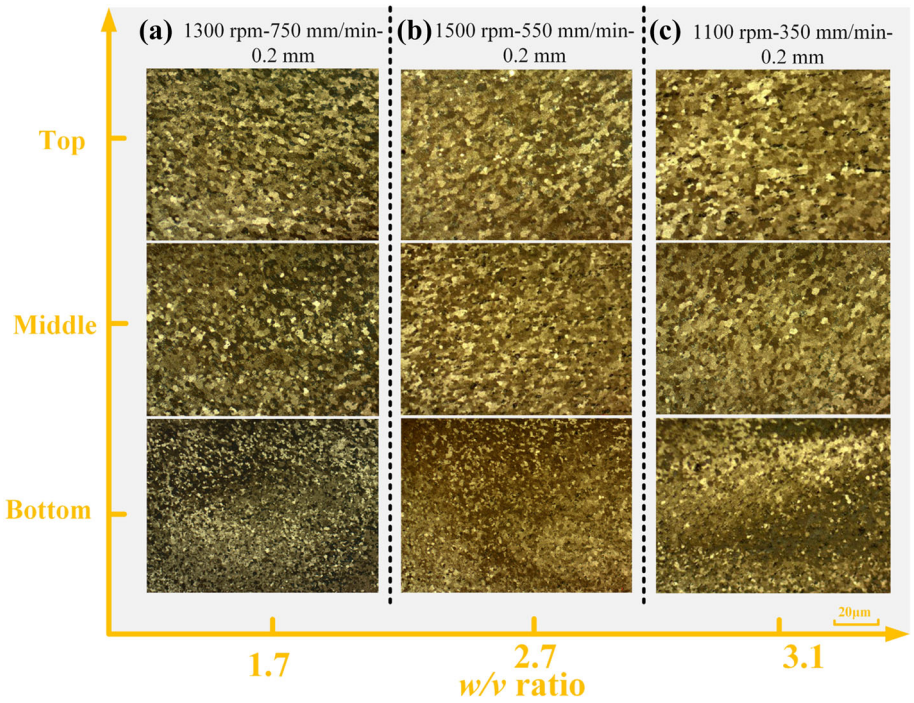

Fig. 6 Grains at SZ top, middle and bottom: **a** 1300 rpm-750 mm/min-0.2 mm, **b** 1500 rpm-550 mm/min-0.2 mm and **c** 1100 rpm-350 mm/min-0.2 mm

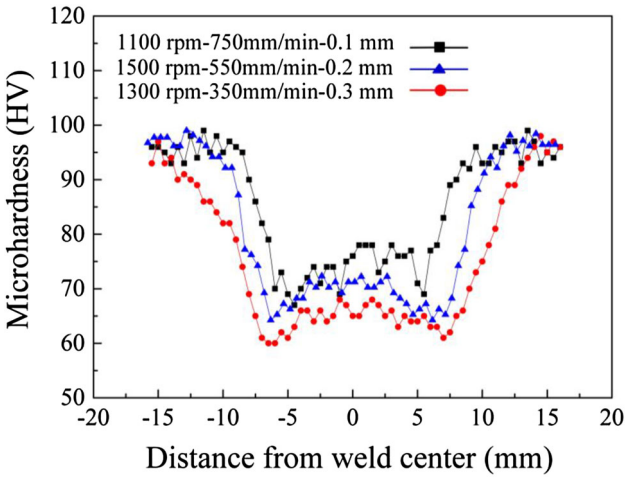

Fig. 7 Microhardness distributions of the joints under different parameter combinations

as well as the joint with highest tensile strength (1500 rpm, 550 mm/min and 0.2 mm). The microhardness distributions under different parameter combinations present a similar change trend. The microhardness first decreases from BM to the transition region between the HAZ and TMAZ and then has a slight increase from the transition region to SZ, resulting in a W-shaped curve. The softening degree of the joint increases with the increase of peak temperature. The average microhardness in the SZ with the experiment No. 3, 8 and 4 in Table 2 are 74 HV, 68 HV and 64 HV, respectively. According to the Hall–Petch relationship, smaller the grains of material, higher is the microhardness [30]. However, as an age-hardening alloy, the microhardness of the 6005A-T6 alloy is mainly dominated by the precipitated phase [31]. BM is in the state of highest strength, which can be attributed to the metastable precursors of the equilibrium β″ (Mg_5Si_6) phases [32]. During the welding process, the joint peak temperature exceeds the precipitates-evolution temperature (220–250 °C), leading to the dissolution and transformation of precipitated phase and then to the decrease of microhardness. Higher the heat input, higher is the degree of β″ dissolution and the coarser grains, which results in a lower microhardness. Moreover, the increased heat input also leads to an enlarged region with high temperature, which results in the increased width of the softening region. The microhardness distribution in the SZ has an obvious fluctuation under low heat input, and this fluctuation becomes small when it comes to the high heat input. Generally, a high tensile strength is associated with a high microhardness. Although the parameter combination with low heat input is beneficial to the decrease of the softening degree of the joint, it leads to the appearance of internal defects which are detrimental to the joint tensile strength. Therefore, although the joint obtained under the parameter combination of 1100 rpm-750 mm/min-0.1 mm has a relatively high microhardness compared with the joint obtained under the optimum parameter combination (1500 rpm-550 mm/min-0.2 mm), its tensile strength is relatively low. The optimum parameter combination provides a relatively high microhardness under the precondition of no defect appearance.

4.5 Fracture Locations and Morphologies

The joints obtained under different parameter combinations fracture at different locations. The joints with low peak temperature mainly fracture in the SZ due to the cavity defect resulting from the insufficient material flow (Fig. 8a). However, the joints with relatively high peak temperature fracture in the transition region between the TMAZ and HAZ (Fig. 8b), corresponding to the lowest microhardness location. During the welding process, the TMAZ and HAZ experience a heating process, resulting in the dissolution of strengthening precipitates. Therefore, the microhardness in these zone deceases compared with BM. The severe deformation in the TMAZ leads to an effect of strain hardening, resulting in the increase of microhardness. Therefore, the complex combined effect from the thermal cycle and plastic deformation induces that the microhardness in the TMAZ is higher than that in the HAZ adjacent to the TMAZ, and the weakest location of the joint is formed in the transition region between the TMAZ and HAZ. The material at AS undergoes bigger shear stress and higher peak temperature compared with that at RS, which leads to the fact that plastic deformation of material in the TMAZ of AS is more severe than that of RS [33]. Therefore, the microstructural heterogeneity between TMAZ and HAZ is higher at AS. The strain concentration is prone to appear at the region with higher microstructural heterogeneity under the tensile load due to the difference in the stress–strain properties between the materials in the TMAZ and HAZ, which easily leads to the initiation of fracture crack [34]. Hence, the specimens are prone to fracture at AS.

The fracture surface located in the transition region is covered with numerous dimples with different sizes, presenting a ductile fracture mode (Fig. 8c). The coarse second phases are visible in some dimples. According to the literatures of Dong et al. [32] and Lee et al. [16], the second phase is the precipitate of β′ ($Mg_{1.7}Si$) deriving from the transformation of β″. The dimples on the fracture surface located in the SZ are relatively small due to the finer microstructure in the SZ (Fig. 8d). The high peak temperature in the SZ leads to the dissolution of precipitated phase and the high cooling rate of the FSW process restrains the occurrence of reprecipitation [15]. Therefore,

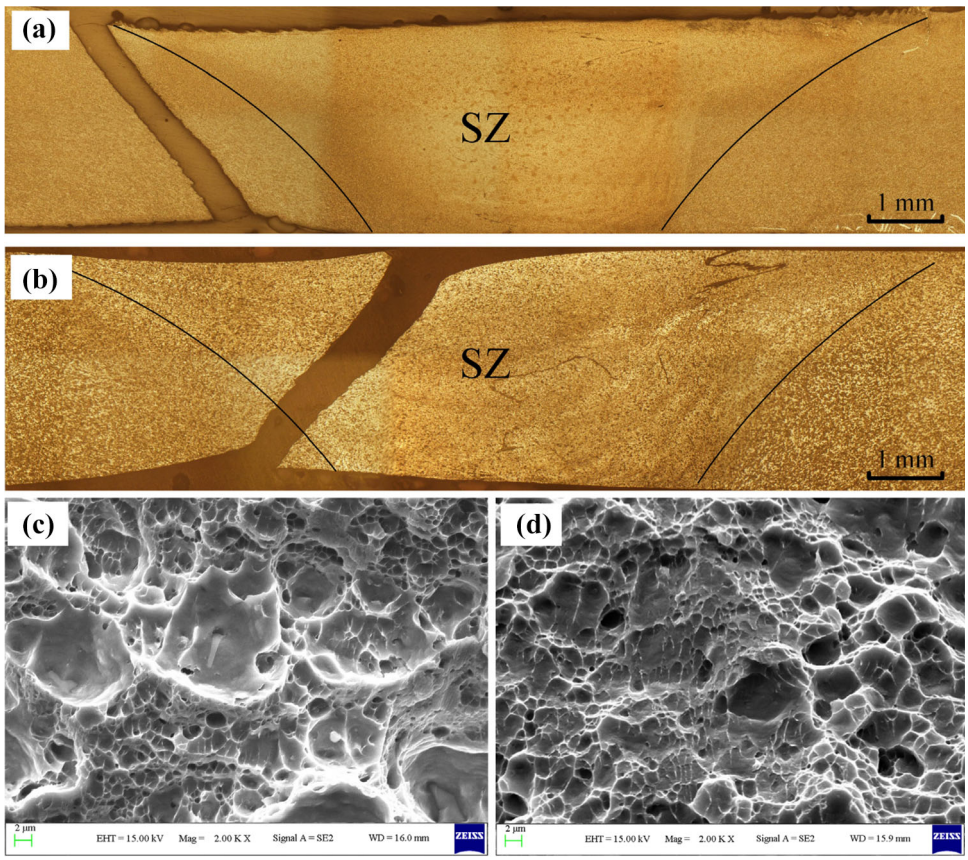

Fig. 8 Fracture locations in **a** transition region between TMAZ and HAZ and **b** SZ; Fracture morphologies in **c** transition region between TMAZ and HAZ and **d** SZ

no coarse precipitated phase is observed in the dimples (Fig. 8d).

5 Conclusions

1. The optimum process parameters are obtained by Taguchi method, and the joint maximum tensile strength is 239.6 MPa reaching 84% of that of the BM.
2. The ANOVA and S/N results indicate that the investigated control factors of rotating speed, welding speed and plunge depth have a significant influence on the joint tensile strength and, respectively, contribute about 53%, 26% and 17% to the overall contribution.
3. The tensile strength of FSW joint is associated with the welding thermal cycle and material flow. The parameter combination with low heat input easily causes the appearance of internal defects, while that with high heat input leads to the increase of softening degree. The optimum parameter combination not only avoids the internal defects but also makes the joint to have a relatively low softening degree.
4. The joints without internal defect mainly fracture in the transition region between TMAZ and HAZ due to the lowest microhardness and possess a ductile fracture mode.

Acknowledgements This work is supported by the National Natural Science Foundation of China (No. 51705339) and the Education Department Foundation of Liaoning Province (No. L201749)

References

1. Niu P, Li W, Zhang Z, and Yang X, *J Mater Sci Technol* **33** (2017) 987.
2. Huang Y, Meng X, Xie Y, Wan L, Lv Z, Cao J, and Feng J, *Compos Part A* **105** (2018) 235.
3. Aydin H, Tutar M, Durmus A, Bayram A, and Sayaca T, *Trans Indian Inst Met* **65** (2012) 21.
4. Ji S D, Meng X C, Li Z W, Ma L, and Gao S S, *Int J Adv Manuf Technol* **84** (2016) 2391.
5. Liu H J, Fujii H, Maeda M, and Nogi K, *J Mater Process Technol* **142** (2013) 692.
6. Besel M, Besel Y, Mercado U A, Kakiuchi T, and Uematsu Y, *Int J Fatigue* **77** (2015) 1.
7. Jaiganesh V, and Sevvel P, *Trans Indian Inst Met* **68** (2015) 99.
8. Chen Y, Liu H, and Feng J, *Mater Sci Eng A* **420** (2006) 21.
9. Li W, Fu T, Hütsch L, Hilgert J, Wang F F, dos Santos J F, and Huber N, *Mater Des* **64** (2014) 714.
10. Ramanjaneyulu K, Reddy G M, and Rao A V, *Trans Indian Inst Met* **67** (2014) 769.

11. Meng X, Xu Z, Huang Y, Xie Y, Wang Y, Wan L, Lv Z, and Cao J, *Int J Adv Manuf Technol* **94** (2018) 1253.
12. Harikrishna K L, Dilip J J S, Choudary K R, Rao V V S, Rao S R K, Ram G D J, Sridhar N, and Reddy G M, *Trans Indian Inst Met* **63** (2010) 807.
13. Meng X, Gao S, Ma L, Yue Y, Xiao H, *Eng Rev* **36** (2016) 107.
14. Ji S D, Meng X C, Liu J G, Zhang L G, and Gao S S, *Mater Des* **62** (2014) 113.
15. Dong P, Li H M, Sun D Q, Gong W B, and Liu J, *Mater Des* **45** (2013) 524.
16. Lee W B, Yeon Y M, and Jung S B, *Mater Sci Technol* **19** (2003) 1513.
17. Simar A, Bréchet Y, de Meester B, Denquin A, and Pardoen T, *Mater Sci Eng A* **486** (2008) 85.
18. Bilici M K, Yükler A İ, and Kurtulmuş M, *Mater Des* **32** (2011) 4047.
19. Anawa E M, and Olabi A G, *J Mater Process Technol* **204** (2008) 22.
20. Javadi Y, Sadeghi S, and Najafabadi M A, *Mater Des* **55** (2014) 27.
21. Yang W H, and Tarng Y S, *J Mater Proc Technol* **84** (1998) 122.
22. Qian J, Li J, Sun F, Xiong J, Zhang F, and Lin X, *Scr Mater* **68** (2013) 175.
23. Li W, Jiang R, Zhang Z, and Ma Y, *Adv Eng Mater* **15** (2013) 1051.
24. Hao D D, and Tra T H, *Arch Mater Sci Eng* **77** (2016) 58.
25. Jamalian H M, Ramezani H, Ghobadi H, Ansari M, Yari S, and Givi M K B, *J Manuf Process* **21** (2016) 180.
26. Huang Y X, Meng X, Zhang Y, Cao J, and Feng J, *J Mater Process Technol* **250** (2017) 313.
27. Ramulu P J, Narayanan R G, Kailas S V, and Reddy J, *Int J Adv Manuf Technol* **65** (2013) 1515.
28. Liu Z, Ji S, Meng X, *J Mater Eng Perform* **27** (2018) 1404.
29. Fattah-alhosseini A, Taheri A H, and Keshavarz M K, *Trans Indian Inst Met* **69** (2016) 1423.
30. Hall E, *Proc Phys Soc Sect B* **64** (1951) 747.
31. Simar A, Bréchet Y, Meester B D, Denquin A, and Pardoen T, *Mater Sci Eng A* **486** (2008) 85.
32. Dong P, Sun D, and Li H, *Mater Sci Eng A* **576** (2013) 29.
33. Ji S D, Meng X C, Ma L, Gao S S, *Int J Adv Manuf Technol* **87** (2016) 3051.
34. He C, Liu Y, Dong J, Wang Q, Wagner D, Bathias C, *Int J Fatigue* **82** (2016) 379.